

Large quantum fluctuations in the strongly coupled spin- $\frac{1}{2}$ chains of green diopside $\text{Cu}_6\text{Si}_6\text{O}_{18}\cdot 6\text{H}_2\text{O}$

O. Janson,* A. A. Tsirlin, M. Schmitt, and H. Rosner[†]*Max-Planck-Institut für Chemische Physik fester Stoffe, D-01187 Dresden, Germany*

(Received 22 April 2010; revised manuscript received 18 June 2010; published 22 July 2010)

We unravel the magnetic nature of the mineral diopside $\text{Cu}_6\text{Si}_6\text{O}_{18}\cdot 6\text{H}_2\text{O}$ and show that strong quantum fluctuations can be realized in an essentially framework-type spin lattice of coupled chains, thus neither frustration nor geometric low dimensionality are prerequisites. We present a microscopic magnetic model for the green diopside. Based on full-potential density-functional theory calculations, we find two relevant couplings in this system: an antiferromagnetic coupling J_c , forming spiral chains along the hexagonal c axis, and an interchain ferromagnetic coupling J_d within structural Cu_2O_6 dimers. To refine the J_c and J_d values and to confirm the proposed spin model, we perform quantum Monte Carlo simulations for the diopside spin lattice. The derived magnetic susceptibility, the magnetic ground state, and the sublattice magnetization are in remarkably good agreement with the experimental data. The refined model parameters are $J_c=78$ K and $J_d=-37$ K with $J_d/J_c \approx -0.5$. Despite the apparent three-dimensional features of the spin lattice and the lack of frustration, strong quantum fluctuations in the system are evidenced by a broad maximum in the magnetic susceptibility, a reduced value of the Néel temperature $T_N \approx 15$ K $\ll J_c$, and a low value of the sublattice magnetization $m=0.55 \mu_B$. All these features should be ascribed to the low coordination number of 3 that outbalances the three-dimensional nature of the spin lattice.

DOI: [10.1103/PhysRevB.82.014424](https://doi.org/10.1103/PhysRevB.82.014424)

PACS number(s): 71.20.Ps, 75.10.Pq, 75.30.Cr, 75.30.Et

I. INTRODUCTION

Since ancient times, emerald has been one of the most rare and treasured gemstones because of its bright and brilliant green color. However, by far not all gemstones that were collected as emeralds or varieties of it were indeed emeralds—many of them later appeared to be specimens of green diopside (see Fig. 1). We attempt in the present study to unravel the also controversially debated magnetic properties based on the paradigm of quantum mechanics and modern electronic-structure theory.

Diopside is a copper silicate mineral forming remarkably large shiny green rhombohedral crystals. Scientifically, it was first described and named by René-Just Haüy in the famous “*Traité de Minéralogie*” in 1801.¹ Vauquelin, as reported in Ref. 1, found that diopside was a copper mineral

containing silicate and, erroneously, carbonate anions. Only later, pure diopside samples were analyzed and recognized as copper silicate with crystal water.²

Structure determination showed that hydrous green diopside with the chemical composition $\text{Cu}_6\text{Si}_6\text{O}_{18}\cdot 6\text{H}_2\text{O}$ is a cyclosilicate with six-membered Si_6O_{18} rings (compare Fig. 1, left) crystallizing in the space group $R\bar{3}$ (SG 148).^{3,4} These rings are interconnected by Cu^{2+} ions with a characteristic local environment of elongated octahedra formed by oxygen atoms. The Cu-O bond lengths in this arrangement are typical with about 1.96 Å for the distorted equatorial plane of the octahedra and a bit larger than usual (between 2.5 and 2.65 Å) for the apical oxygens belonging to the crystal water. Due to the sharing of the octahedral O-OH₂ edges, the magnetic Cu^{2+} ions form helical chains around the

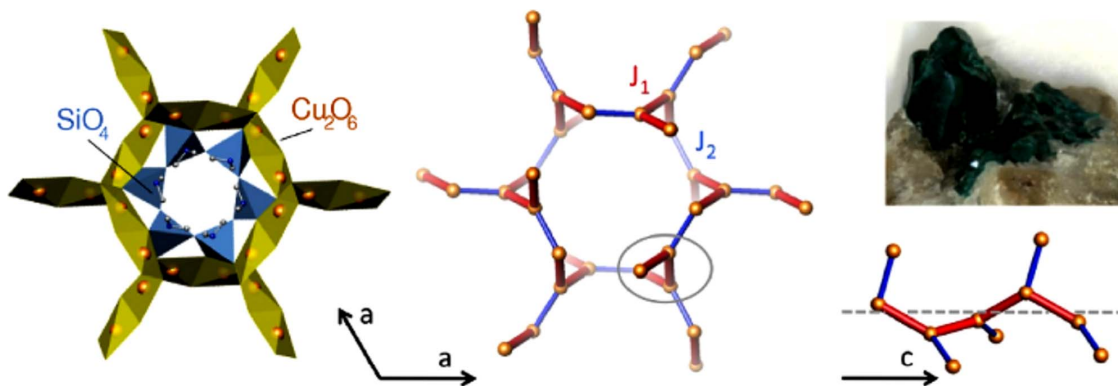


FIG. 1. (Color online) Left: crystal structure of the green diopside. The Cu_2O_6 dimers (light) form a 3D network with isolated Si_6O_{18} rings (dark) inside the channels. Middle: the magnetic model of the green diopside. Cu atoms are depicted as orange spheres, other atoms are not shown. The leading antiferromagnetic coupling J_c (red thick lines) forms spiral chains running along c perpendicular to the projection plane. The ferromagnetic coupling J_d (blue thin lines) within the structural Cu_2O_6 dimers couples the chains into a three-dimensional framework. Right: section of the spiral chain along c (bottom) and a natural sample of green diopside grown on calcite (top).

threefold axis along c (see Fig. 1). Thus, each Cu atom has two Cu neighbors along these chains and another Cu neighbor with which it forms an edge-shared Cu_2O_6 dimer that connects two adjacent spiral chains (see Fig. 1).

The magnetic properties of green diopside have been investigated in some experimental studies.^{4–8} Although these studies yield quantitatively slightly varying results, likely also related to diopside samples originating from different locations, they essentially converge in the description of diopside as an antiferromagnet with a rather low Néel temperature ($T_N \sim 15$ K) compared to the antiferromagnetic (AFM) Curie-Weiss temperature of about 45 K. The ordered magnetic moment ($m=0.55 \mu_B$) is drastically reduced with respect to the saturation moment of about $1 \mu_B$ for Cu^{2+} . Together with the broad maximum in the measured magnetic susceptibility,^{7,9} this puts the compound in the family of spin- $\frac{1}{2}$ quantum magnets that can be described successfully in many cases by the isotropic Heisenberg model,

$$\hat{H} = \sum_{\langle ij \rangle} J_{ij} \hat{S}_i \cdot \hat{S}_j, \quad (1)$$

at least for spin excitations. Here, J_{ij} represents the exchange interaction per bond between spins located at the lattice sites i and j .

Although this model looks deceptively simple at the first glance, neither its solution for a seemingly ordinary situation nor the assignment of appropriate exchange integrals J_{ij} for a specific material are trivial in any way. It is obvious that the crystal structure of a compound is the key to understand its magnetic properties. On the other hand, an assignment of interaction parameters solely based on structural considerations can be completely misleading, such as in the case of $(\text{VO})_2\text{P}_2\text{O}_7$.^{10,11} In recent years, even careful investigations based on accurate experimental data, but within a limited spectrum of methods, have suggested controversially discussed magnetic models for several compounds. A prominent example for this problem are the two closely related spin- $\frac{1}{2}$ J_1 - J_2 chain compounds Li_2CuO_2 and LiCu_2O_2 , for which consensus about their location in the magnetic phase diagram was established only recently.^{12–18}

Thus, to establish the appropriate magnetic model for a new, complex material, the application of independent methods seems of crucial importance. In particular, the search for the relevant sector in the phase diagram can largely benefit from a detailed microscopic analysis based on modern band-structure theory^{17,19,20} in combination with numerical methods to solve subsequently the corresponding Heisenberg Hamiltonian, at least in an approximate way.^{21,22}

In particular, for green diopside a magnetic model with AFM nearest-neighbor coupling J_c along the spiral chains (see Fig. 1, middle) and AFM coupling J_d within the structural Cu_2O_6 dimers was suggested²³ on empirical grounds and evaluated using quantum Monte Carlo (QMC) simulations to fit the experimental magnetic susceptibility. The authors of Ref. 23 place the compound in proximity to a quantum critical point due to a competition between chainlike ordering along c and magnetic dimer formation caused by the AFM J_d . In contrast to Ref. 23, the results of our microscopic study place the compound in a different region of the

phase diagram and assign the strong quantum fluctuations and the related magnetic properties to the small coordination number of the spin lattice.

II. METHODS

Electronic-structure calculations were performed using the full-potential nonorthogonal local-orbital minimum basis scheme FPLO9.00–33.²⁴ For the scalar relativistic calculations within the local-density approximation (LDA) the exchange and correlation potential of Perdew and Wang was chosen.²⁵ A well-converged k mesh of $8 \times 8 \times 8$ points was used for LDA calculations. Wannier functions (WF) were calculated for the antibonding Cu $3d_{x^2-y^2}$ states. Strong correlations are treated in a mean-field way within the local spin density approximation (LSDA)+ U approach.²⁶ For the double-counting correction (DCC) we applied the two limiting cases: around-the-mean-field (AMF) approach and the fully localized limit (FLL).²⁷ The on-site Coulomb repulsion U_{3d} was varied within the physically reasonable ranges: $U_{3d} = 5.5$ – 7.5 eV for AMF and $U_{3d} = 6.5$ – 9.5 eV for FLL. The intra-atomic Hund's coupling J_{3d} was fixed to 1 eV. To allow for various spin-ordering arrangements, the original hexagonal symmetry was reduced to the space group $P1$. For the LSDA+ U calculations, we used k meshes of $4 \times 4 \times 4$ points. The calculations were carefully checked for convergence with respect to the k mesh. For the structural input, we used crystallographic data from Ref. 4.

QMC simulations were performed using the programs `looper` and `dirloop_sse` of the software package ALPS.²⁸ The magnetic susceptibility was simulated for $N=10\,752$ sites clusters containing 256 coupled chains of 42-sites each. In the temperature range $T/J_c=0.15$ – 4.50 , we used 25 000 sweeps for thermalization and 300 000 sweeps after thermalization. The resulting statistical errors ($<0.1\%$) are far below the experimental inaccuracy. To evaluate the dependence of the static structure factor on the cluster size, we performed a series of simulations starting with a $N=24$ -sites cluster and consequently increasing it up to $N=8232$ -sites. Magnetization curves were simulated on $N=1536$ -sites clusters at $T=0.025J_c$ using 50 000 sweeps for thermalization and 500 000 sweeps after thermalization. Statistical errors did not exceed 0.5%.

The experimental data were collected on a natural sample of green diopside. A green transparent crystal was mechanically detached from the calcite matrix and used for magnetic measurements without alignment in the magnetic field. The magnetic susceptibility was measured with a Quantum Design MPMS superconducting quantum interference device in the temperature range 2–380 K in applied fields up to 5 T.

III. RESULTS

A. Electronic structure and magnetic model

The electronic structure of the green diopside was calculated within the LDA. The atom-resolved density of states (DOS) is depicted in Fig. 2. The width of the valence band is about 10 eV, similar to other cuprates. States at the Fermi level evidence a metallic spectrum in contrast to the green

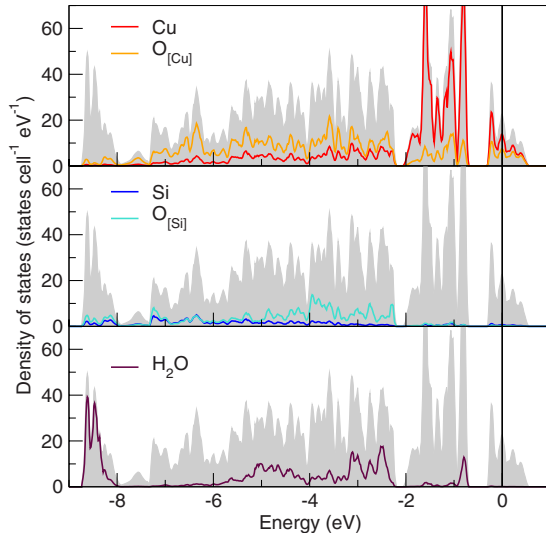


FIG. 2. (Color online) Total and atom-resolved LDA density of states for the green diopside. The antibonding Cu-O $dp\sigma$ states form a well-separated band complex at the Fermi level.

transparent crystals indicating an insulating behavior. This well-known shortcoming of the LDA approach originates from the underestimation of the strong Coulomb repulsion in the Cu $3d$ shell. The insulating ground state (GS) can be restored by adding the missing part of correlation (i) via mapping onto a Hubbard model or (ii) in a mean-field way by LSDA+ U calculations. In this study, both approaches are used.

Despite the incorrect description of the ground state, LDA is known as a reliable tool for the evaluation of relevant orbitals and couplings. We start the analysis from the highest lying states of the valence band. The well-separated band complex at the Fermi level is half filled and formed by antibonding Cu-O $dp\sigma$ states. The energy range between -0.5 and -2 eV is dominated by nonbonding O and Cu states. At lower energies, around -2 eV, states of the SiO_4 tetrahedra and H_2O appear. The sizable H_2O contribution originates from the apical position of the crystal water in the distorted $\text{CuO}_4(\text{H}_2\text{O})_2$ octahedra and thus rather short Cu- $\text{O}_{\text{H}_2\text{O}}$ distances of 2.51 and 2.66 Å.

Typical for cuprates, the magnetic properties of the green diopside are ruled by the half-filled antibonding Cu-O $dp\sigma$ band complex at the Fermi level. The width of this complex W can be used as a rough estimate for the leading couplings. Thus, $W=0.8$ eV for the green diopside is comparable to related systems such as $\text{Li}_2\text{ZrCuO}_4$ (buckled edge-shared chains, $W=0.5$ eV),²⁹ $\text{Cu}_2(\text{PO}_3)_2\text{CH}_2$ (distorted dimers, $W=1$ eV),³⁰ or kagellite (kagome lattice of corner-shared plaquettes with a Cu-O-Cu bond angle of about 107° , $W=0.9$ eV) (Ref. 21) but it is strongly reduced compared to Sr_2CuO_3 (chains of corner-shared plaquettes, $W=2.5$ eV) (Ref. 31) or SrCuO_2 (zigzag chains of edge-shared plaquettes, $W=2$ eV).³² Based on such simplified comparative analysis, we can conjecture the leading couplings in diopside to be on the order of 100 K.

The orbitals which are relevant for the magnetism can be evaluated by a projection onto a set of local atomic orbitals.

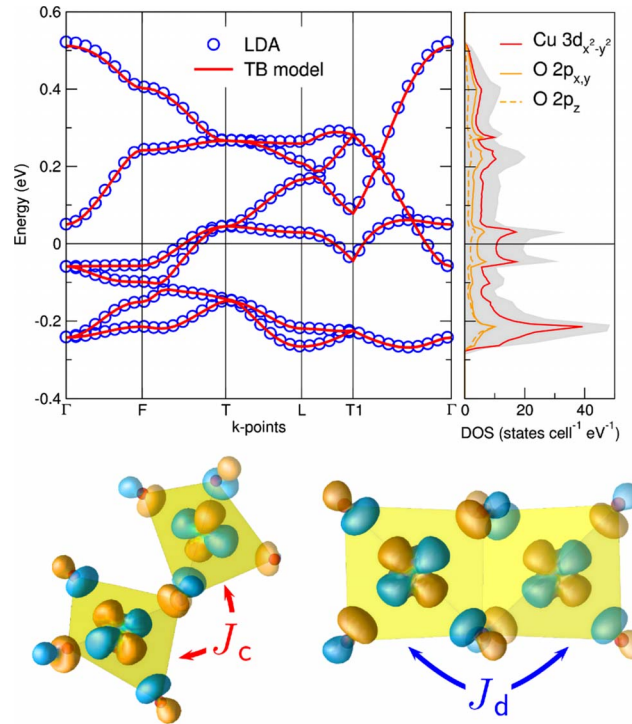


FIG. 3. (Color online) Top: comparison of the antibonding $dp\sigma$ bands from the LDA calculation and the tight-binding model (left) together with the orbital-resolved density of states (right). Bottom: Cu-centered Wannier functions superimposed upon the leading superexchange pathways.

For each plaquette, one of the Cu-O bonds and a direction perpendicular to the plaquette are considered as local x and z coordinate axes, respectively. This way, we find that Cu states in the $dp\sigma$ band complex have nearly pure Cu $3d_{x^2-y^2}$ character (see Fig. 3, right), although the plaquettes forming the structural Cu_2O_6 dimers are considerably distorted. On contrary, the orbital-resolved DOS for the O states shows a mixture of $2p_{x,y}$ and $2p_z$ states. This mixing is caused by a noncoplanar arrangement of the neighboring dimers, sharing a common O atom.³³ Thus, although the O $2p_z$ contributions are unusually high and seemingly hint at sizable O $2p_\pi$ contributions, the states around the Fermi energy are clearly dominated by Cu-O $dp\sigma$ states. Since the number of bands forming the band complex coincides with the number of plaquettes in the unit cell, magnetic properties of the compound can be described by an effective one-orbital tight-binding (TB) model.

In case of the green diopside, the evaluation of its magnetic model from simple geometric considerations, based on the crystal structure only, is difficult due to a complex three-dimensional (3D) coupling between the structural dimers. To develop a magnetic model of the compound from microscopic grounds, the six bands at the Fermi level were mapped onto an effective one-orbital TB model parametrized with transfer integrals t_{ij} . The WF technique yields an unambiguous solution of this six-band fitting problem. The resulting fit shows a perfect description of the LDA band structure (Fig. 3).

Only two of the resulting transfer integrals t_{ij} are relevant: $t_c=126$ meV (the subscript c stands for “chain”), running

along the spirals of dimers (in the c direction), and $t_d = 104$ meV, the intradimer coupling (compare Fig. 1, middle). Other hoppings (except for the hopping $t_{ic} = 24$ meV between the spirals) are smaller than 20 meV. To restore the insulating ground state, we map the TB model onto a Hubbard model considering an effective (one band) Coulomb repulsion $U_{\text{eff}} = 4$ eV. For the strongly correlated limit at half filling, both well justified for the green diopside, the lowest-lying (magnetic) excitations can be efficiently described by a Heisenberg model. This way, the resulting magnetic exchange can be derived using the second-order perturbation-theory expression $J_{ij}^{\text{AFM}} = 4t_{ij}^2/U_{\text{eff}}$. Since the original TB model is a one-orbital model, only the AFM contribution to the total magnetic exchange is accounted for in this approach. Thus, the resulting AFM contributions for the leading couplings are $J_c^{\text{AFM}} = 184$ K and $J_d^{\text{AFM}} = 125$ K. Since exchange integrals J_{ij}^{AFM} are proportional to t_{ij}^2 , all further exchanges are smaller than 7 K (less than 4% of the leading exchange) and can be neglected in first place.

Due to their close vicinity to 90° , the intradimer Cu-O-Cu bond angle of 97.4° and interdimer angle of 107.6° call for a careful estimation of the ferromagnetic (FM) contributions to the total exchange integrals, neglected in the effective one-orbital TB-model approach presented above. Thus, we performed LSDA+ U calculations of magnetic supercells with various collinear spin arrangements. The mapping of total-energy differences onto a classical Heisenberg model results in an AFM exchange along the spiral chains $J_c = 110$ K and a FM intradimer exchange $J_d = -66$ K for a typical value of $U_{3d} = 6.5$ eV within the AMF DCC scheme.³⁴

In agreement with the expectations according to the Goodenough-Kanamori-Anderson rules,^{35–37} the LSDA+ U calculations evidence considerable FM contributions to both leading exchange integrals J_c and J_d . The total value of J_c is strongly reduced compared to the estimate from the one-orbital model ($J_c^{\text{AFM}} = 184$ K), yielding $J_c^{\text{FM}} = -74$ K and $J_c = 110$ K. For J_d , the closer proximity of the Cu-O-Cu angle to 90° leads to an even larger FM contribution $J_d^{\text{FM}} = -191$ K which exceeds the AFM part $J_d^{\text{AFM}} = 125$ K, resulting in a significantly FM total coupling $J_d = -66$ K within the structural dimers.

Since the choice of DCC is nontrivial and can have a large impact on the resulting exchange parameters, we compare the AMF and FLL results.^{22,38} For the green diopside, we find that both DCC schemes yield similar couplings (Fig. 4). The only apparent difference is related to the values of U_{3d} : for FLL, about 2 eV larger U_{3d} values are required in order to obtain the same exchange integrals as AMF. The FM nature of J_d is robust with respect to the choice of U_{3d} and the DCC scheme.

Although the qualitative microscopic model is well justified by varying the U_{3d} parameter in a rather wide range, the strong dependence of the resulting exchange integrals on U_{3d} impedes an accurate estimation of the absolute size and the ratio of the two couplings. In the next section, we refine the values of the exchange integrals by fitting the experimental data.

To summarize the microscopic analysis, we obtain a model with two leading interactions: an AFM J_c running along the spiral (in the c direction) and an FM J_d inside the

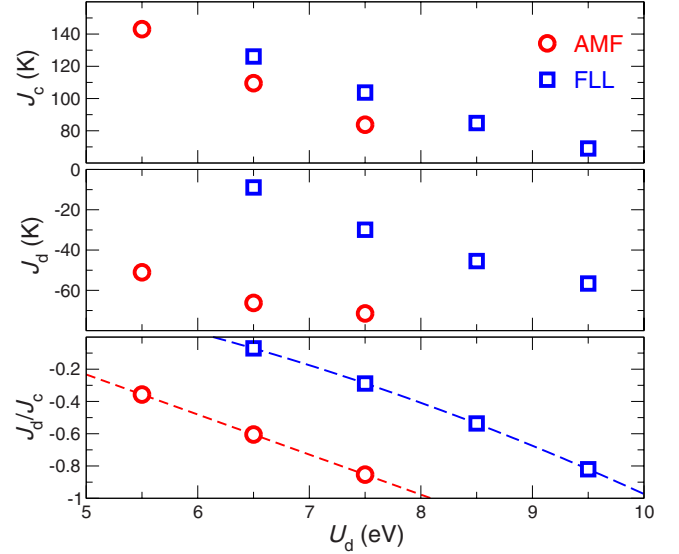


FIG. 4. (Color online) Results of total-energy LSDA+ U calculations: the leading exchange integrals (J_c and J_d) and their ratio as a function of the on-site Coulomb repulsion U_{3d} for AMF and the FLL double-counting correction schemes.

structural Cu_2O_6 dimers. We should note that a related magnetic model was proposed in Ref. 23. It is based on the same relevant exchange interactions but includes an AFM intradimer coupling J_d in contrast to the FM nature of this coupling in our model. Remarkably, a model very similar to ours has been proposed for the dehydrated, black species of diopside $\text{Cu}_6\text{Si}_6\text{O}_{18}$.⁷ This issue will be discussed in Sec. IV.

B. Experimental results and model simulations

To challenge our model with respect to the experimental data, we measured the magnetic susceptibility of the green diopside (Fig. 5) and used neutron-diffraction results from previous studies.⁴ Our susceptibility data are in good agreement with the earlier reports^{9,23} and show a broad maximum at 50 K along with the magnetic-ordering anomaly, evidenced by a kink at $T_N \approx 15$ K. We do not observe any appreciable field dependence up to 5 T. Above 200 K, the susceptibility can be fitted to the Curie-Weiss law, modified with an additional temperature-independent contribution χ_0 , responsible for core diamagnetism and Van Vleck paramagnetism. The Curie-Weiss fit leads to $\chi_0 = -7.2 \times 10^{-5}$ emu/mol, the effective magnetic moment $\mu_{\text{eff}} = 1.99 \mu_B$ ($g = 2.30$), and the Weiss temperature $\theta = 43$ K. Note that the susceptibility below T_N depends on the crystal orientation in the magnetic field and can only be treated within an anisotropic model. In contrast, the magnetic behavior in the paramagnetic regime (above T_N) is isotropic: the susceptibility simply scales due to different g values along different crystal directions.³⁹ Since our microscopic study yields the exchange integrals of the isotropic (Heisenberg) Hamiltonian, we restrict our comparison to the data above T_N .

Density-functional theory (DFT) calculations evidence two relevant interactions—the AFM intrachain exchange J_c and the FM intradimer (interchain) exchange J_d . Below, we

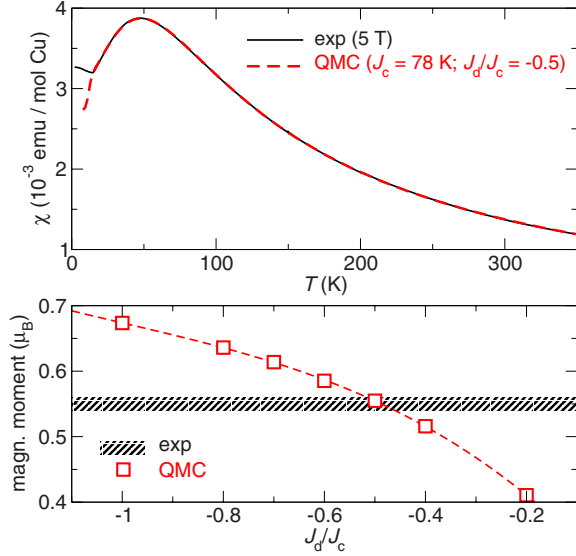


FIG. 5. (Color online) Top: the QMC fit to the experimental magnetic susceptibility (per mol Cu). Bottom: QMC results for the ordered magnetic (sublattice) moment as a function of the J_d/J_c ratio. The experimental value from the neutron diffraction (Ref. 4) with a standard deviation is depicted by a striped bar.

will compare this model to the experimental results and refine the values of the leading exchange integrals. Since the microscopic model is well justified qualitatively (relevant couplings and their sign), its internal parameters J_c and J_d can be refined by varying them in a reasonable range and subsequently simulating the thermodynamic behavior for a given J_d/J_c ratio.

A method for simulations should be certainly consistent with the spin model. Since the two relevant couplings in diopside form a nonfrustrated, formally three-dimensional spin lattice, QMC simulations are natural and, probably, the only feasible choice. Therefore, we perform QMC simulations for the relevant parameter range $-1 \leq J_d/J_c \leq -0.2$ of the J_c - J_d model.

Simulations of the Heisenberg Hamiltonian yield a reduced magnetic susceptibility χ^* which is related to the experimentally measured χ by the expression,

$$\chi(T) = \frac{N_A g^2 \mu_B^2}{k_B J_c} \chi^* \left(\frac{T}{k_B J_c} \right) + \frac{C_{\text{imp}}}{T} + \chi_0, \quad (2)$$

where N_A , k_B , and μ_B stand for the Avogadro constant, the Boltzmann constant, and the Bohr magneton, respectively, g is the Lande factor, C_{imp} is the Curie constant to account for possible impurity and defect contributions, and χ_0 is a temperature-independent term, similar to the Curie-Weiss fit.

Although a fit to $\chi(T)$ is commonly regarded as a sensitive probe for internal parameters of a magnetic model,⁴⁰ we find that the ratio J_d/J_c can be varied in a rather wide range ($-0.8, \dots, -0.4$) yielding a very good fit to the experimental data above T_N .⁴¹ To improve our refinement of J_d/J_c , we have to address the magnetic-ordering temperature T_N , which can be traced by a clear kink in the simulated curves. The reference to T_N yields J_d/J_c close to -0.5 . The respective fit

is shown in Fig. 5 (top). The resulting $J_c = 78$ K agrees well with the DFT estimates: 110 K for $U_{3d} = 6.5$ eV within the AMF scheme ($J_d/J_c = -0.6$) and even better with 85 K at $U_{3d} = 8.5$ eV from the FLL scheme ($J_d/J_c = -0.55$). Moreover, $g = 2.26$ and $\chi_0 = -6.9 \times 10^{-5}$ emu/mol are consistent with the estimates from the Curie-Weiss fit ($g = 2.30$, $\chi_0 = -7.2 \times 10^{-5}$ emu/mol, respectively).

For a further test of our model, we will address its ground-state properties. First, the propagation vector \vec{q} of the AFM ordered GS coincides with the experimentally observed $\vec{q} = (0, 0, \frac{2}{3}\pi)$ (Ref. 4) in the whole range $-1 \leq J_d/J_c \leq -0.2$. In this GS, the neighboring spins along the spiral chains (J_c) align antiferromagnetically while the ordering within the edge-shared dimers (J_d) is FM. This justifies the validity of our microscopic model but does not allow for a more accurate refinement of the proposed value for the J_d/J_c ratio. For a further comparison, we use the sublattice magnetization (m) that has been previously estimated in neutron diffraction experiments⁴ and amounts to $0.55(1) \mu_B$.⁴²

Unfortunately, the theoretical estimation of m is not straightforward for two reasons. First, the simulations do not yield the magnetic moment in the ordered state directly. Instead, it can be calculated from the static structure factor or from spin correlations. Second, the spin lattice of the green diopside is geometrically 3D, thus sizable finite-size effects are expected even for large clusters. To account for these effects, we use the general procedure from Ref. 45 and estimate the magnetic moment m using finite-size scaling of the static structure factor, taken for the propagation vector of the ordered structure. The results of the simulations for various J_d/J_c ratios are shown in Fig. 5 (bottom). Remarkably, the theoretical m for $J_d/J_c = -0.5$ is in good agreement with the experimental value.

Finally, we can introduce a magnetic field term to our Hamiltonian and simulate the behavior of magnetization M as a function of the reduced magnetic field $0 \leq h^* \leq 5$. Such a simulation could be an additional test for our model since high-field magnetization experiments were recently announced.⁹ Therefore, we simulate $M(h^*)$ curves for $J_d/J_c = -0.5 \pm 0.2$ and scale them using the expression

$$M(H) = M \left(\frac{k_B J_c}{g \mu_B} h^* \right), \quad (3)$$

adopting the J_c and g values from the fits to $\chi(T)$. The resulting curves shown in Fig. 6 have similar shape and only slightly different values of the saturation field.⁴⁶ Therefore, the experimental $M(H)$ dependence is unlikely to facilitate a further refinement of the model parameters due to practical resolution limits at high magnetic fields. In addition, the predicted value of the saturation field remains challenging for present-day experimental facilities.

IV. DISCUSSION

In our model, the spin lattice of the green diopside comprises AFM couplings J_c between the corner-sharing CuO_4 plaquettes and FM couplings J_d between the edge-sharing plaquettes (Fig. 1). This situation is not surprising because

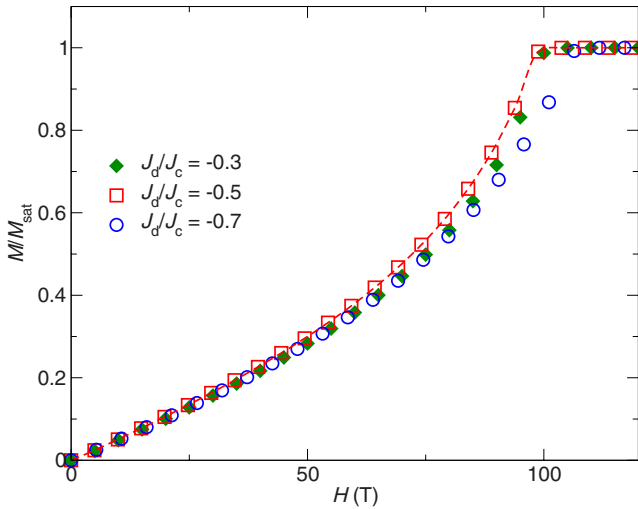


FIG. 6. (Color online) Simulated high-field magnetization curves for three different values of the J_d/J_c ratio. The magnetic field is scaled by adopting the values of J_c and g from the fits to $\chi(T)$.

the corner-sharing connection normally leads to 180° superexchange while the edge-sharing connection corresponds to the Cu-O-Cu angle close to 90° . However, the crystal structure of the green dioptase shows a tiny difference between the superexchange pathways. The twisted configuration of the corner-sharing plaquettes leads to the Cu-O-Cu angle of 107.6° for J_c that is substantially larger than 97.4° for J_d . The smaller angle for J_d still fits to the general trend, predicted by Goodenough-Kanamori-Anderson rules.^{35–37} On the other hand, the green dioptase is very close to the “critical regime” of the Cu-O-Cu superexchange. Then, even a weak structural change could lead to a strong modification of the exchange couplings, making an empirical assignment of the parameter region difficult. For example, the earlier theoretical analysis assumed both J_c and J_d to be AFM.²³ Therefore, we used a quantitative microscopic approach and demonstrated that this empirical assumption is not consistent with the electronic structure of the compound.

To examine whether small changes in the crystal structure may lead to a modification of the microscopic model, the consideration of structurally related compounds is a natural approach. The dehydration transforms the green dioptase into the black dioptase $\text{Cu}_6\text{Si}_6\text{O}_{18}$ that essentially keeps the 3D framework-type crystal structure (Fig. 1) but lacks water molecules. The Cu-O-Cu angles amount to 110.7° and 97.3° for J_c and J_d , respectively.⁴⁷ Thus, based on empirical structural arguments, the signs of the two couplings should persist, while the absolute values are likely increased. This prediction is in line with the experimental data, indicating a large Weiss temperature θ of 180 K (Ref. 7) of the black dioptase compared to $\theta=43$ K in the green dioptase (Sec. III B). In addition, neutron-diffraction studies evidence similar magnetic structures for the black and green dioptase.⁷ On the other hand, a very recent study of black dioptase based on extended Hückel calculations and a one-dimensional fit to the magnetic susceptibility assigns the compound to the family of uniform AFM chains with very weak interchain interactions.⁴⁸

Further examples of the dioptase structure are given by the hydrated and anhydrous Cu germanates $\text{Cu}_6\text{Ge}_6\text{O}_{18}\cdot x\text{H}_2\text{O}$ with $x=0$ and 6. These compounds were previously considered as coupled frustrated spin chains because a sizable next-nearest-neighbor coupling along the spiral chains was assumed.^{49,50} This assumption is rather empirical and mainly motivated by the chemical similarity to the well-known spin-Peierls compound CuGeO_3 with its frustrated spin chains of edge-sharing CuO_4 plaquettes.⁵¹ However, the pronounced difference in the crystal structures strongly impedes a reliable transfer of the well-established magnetic model of the chain compound CuGeO_3 to the Ge-dioptase $\text{Cu}_6\text{Ge}_6\text{O}_{18}$.⁴⁹ Based on the results for the Si dioptase, we would expect sizable AFM J_c , while J_d is either FM or AFM. If the FM and AFM contributions to J_d are close to cancel each other, the interchain coupling is effectively switched off, and long-range couplings along the spiral chains could alter the physics. However, we do not find any frustrating next-nearest-neighbor couplings in the green dioptase. A detailed microscopic study, which is presently underway, aims to check to which extent the J_c - J_d model is applicable for the germanate compounds.⁵²

Taking the green dioptase as an example, we have derived the basic features of the dioptase spin lattice. This spin lattice is unfrustrated, hence we should preclude any references to the frustrated spin chain model, at least for the green dioptase $\text{Cu}_6\text{Si}_6\text{O}_{18}\cdot 6\text{H}_2\text{O}$. It is worth to mention that the dioptase structure does *not* give rise to the star lattice (decorated honeycomb lattice), as it may seem on the first glance.⁵³ Such confusion could arise from a specific projection of the crystal structure, where the spiral chains look like flat frustrated triangles (compare to the middle panel of Fig. 1).

After shortly outlining what the dioptase spin lattice is not, it is more important to establish what it actually is: uniform AFM spin chains aligned along the c direction are arranged on the honeycomb lattice, i.e., each chain is coupled to three neighboring chains, and the system is geometrically 3D (Fig. 1). However, the *total* coordination number is as low as three: each atom has two J_c bonds and one J_d bond only. Thus, the couplings in the ab plane form a kind of a “sparse” honeycomb lattice. The reduction in the coordination number has strong effect on the magnetic properties.

Experimental data for the green dioptase evidence strong quantum fluctuations: the broad susceptibility maximum at $T_{\text{max}}^X/J_c \approx 0.64$, the low Néel temperature ($T_N/J_c \approx 0.2$), and the reduced sublattice magnetization ($0.55 \mu_B$ compared to $1 \mu_B$ for the classical spin- $\frac{1}{2}$ systems). Strong quantum fluctuations are usually observed in low-dimensional and/or frustrated spin systems. For example, the archetypal two-dimensional spin model of the square lattice reveals the susceptibility maximum at $T_{\text{max}}^X/J \approx 1.0$ and a sublattice magnetization of $0.6 \mu_B$.⁴⁵ To reduce the ordering temperature down to $T_N/J=0.2$, a very weak interlayer coupling $J_\perp/J \sim 10^{-4}$ is required.⁵⁴ Thus, the quantum fluctuations in the dioptase spin lattice are even stronger than in the square lattice, despite the 3D geometry.

Quantum fluctuations in a 3D spin system can arise from the magnetic frustration (see Ref. 55 for an instructive example). However, *the dioptase spin lattice is neither low*

dimensional, nor frustrated, hence its quantum behavior has a different origin. We suggest that the long-range magnetic ordering in diopside is impeded by the low-coordination number of the lattice because the low number of bonds reduces the exchange energy that should stabilize the ordered ground state. The diopside lattice can thus be compared to low-dimensional spin systems with similar coordination numbers. For example, the honeycomb lattice having three bonds per site reveals the low sublattice magnetization of $0.54 \mu_B$ and $T_{\max}^X/J \approx 0.7$ (compare to $0.6 \mu_B$ and 1.0 for the square lattice with four bonds per site).⁵⁶ The apparent similarity between the diopside and the honeycomb lattice clearly shows that the coordination number is the actual criterion of the “low dimensionality,” as long as the magnitude of quantum fluctuations (the tendency toward the quantum behavior) is considered. Although this conclusion is a natural consequence of simple energy considerations, it is often overlooked. While neither the diopside crystal structure, nor its spin model look low-dimensional, the essential physics is governed by strong quantum fluctuations, typical for low-dimensional magnets. The above considerations should stimulate further studies of diopside-structure materials and the respective spin model.

V. SUMMARY AND OUTLOOK

Based on density-functional calculations, quantum Monte Carlo simulations, and magnetic measurements we have derived a distinct magnetic model for the natural mineral green diopside $\text{Cu}_6\text{Si}_6\text{O}_{18} \cdot 6\text{H}_2\text{O}$ on a microscopic basis. We have shown that green diopside can be described by a quantum spin- $\frac{1}{2}$ Heisenberg model with two relevant interactions: an nearest-neighbor AFM intrachain coupling $J_c \sim 78$ K within

the spiral chains, running along the crystallographic c direction, and a nearest-neighbor FM intradimer (interchain) coupling $J_d \sim -37$ K within the structural Cu_2O_6 dimers. The simulated temperature dependence of the magnetic susceptibility, the magnetic ground state, the ordering temperature, and the sublattice magnetization for the suggested model parameters are in very good agreement with the experimental data. We conclude that the diopside spin lattice is neither low-dimensional nor frustrated but exhibits large quantum fluctuations due to a small effective coordination number (number of bonds per lattice site) despite the three-dimensional lattice geometry.

Our approach demonstrates the great potential of the combination of modern band-structure methods and numerical simulations for a reliable modeling of the magnetic properties for complex materials. An empirically-based assignment of interaction parameters for structurally complex systems can be easily misleading and restrict studies to inappropriate regions of the magnetic phase diagram.²³ Since minor structural changes may cause drastic changes in the leading magnetic couplings, especially for Cu-O-Cu angles close to 90° , relevant in the diopside family, a detailed comparative study for the hydrous and anhydrous Si- and Ge-diopside compounds is in progress.⁵²

ACKNOWLEDGMENTS

We are grateful to Deepa Kasinathan for enlightening discussions, Marcus Schmidt for providing us with the samples of diopside and Walter Schnelle for supporting the thermodynamical measurements and valuable comments. A.T. acknowledges the funding from Alexander von Humboldt foundation. We also appreciate the invaluable long-time support from SLD 22-04-1950.

*janson@cpfs.mpg.de

†rosner@cpfs.mpg.de

¹R. J. Haüy, *Traité de Minéralogie* (chez Louis, Libraire, rue de Savoie No. 12, Paris, 1801), Vol. 3, pp. 136–141.

²H. Hess, *Ann. Phys. (Leipzig)* **16**, 360 (1829).

³H. G. Heide and K. Boll-Dornberger, *Acta Crystallogr.* **8**, 425 (1955).

⁴E. L. Belokoneva, Y. K. Gubina, J. B. Forsyth, and P. J. Brown, *Phys. Chem. Miner.* **29**, 430 (2002).

⁵R. D. Spence and J. H. Muller, *J. Chem. Phys.* **29**, 961 (1958).

⁶R. E. Newnham and R. P. Santoro, *Phys. Status Solidi* **19**, K87 (1967).

⁷M. Wintenberger, G. André, and M. F. Gardette, *Solid State Commun.* **87**, 309 (1993).

⁸I. A. Kiseleva, L. P. Ogorodova, L. V. Melchakova, and M. R. Bisengalieva, *J. Chem. Thermodyn.* **25**, 621 (1993).

⁹H. Ohta, S. Okubo, N. Souda, M. Tomoo, T. Sakurai, T. Yoshida, E. Ohmichi, M. Fujisawa, H. Tanaka, and R. Kato, *Appl. Magn. Reson.* **35**, 399 (2009).

¹⁰D. C. Johnston, J. W. Johnson, D. P. Goshorn, and A. J. Jacobson, *Phys. Rev. B* **35**, 219 (1987).

¹¹A. W. Garrett, S. E. Nagler, D. A. Tennant, B. C. Sales, and T.

Barnes, *Phys. Rev. Lett.* **79**, 745 (1997).

¹²M. Boehm, S. Coad, B. Roessli, A. Zheludev, M. Zolliker, P. Böni, D. M. Paul, H. Eisaki, N. Motoyama, and S. Uchida, *Europhys. Lett.* **43**, 77 (1998).

¹³W. E. A. Lorenz, R. O. Kuzian, S.-L. Drechsler, W.-D. Stein, N. Wizen, G. Behr, J. Málek, U. Nitzsche, H. Rosner, A. Hiess, W. Schmidt, R. Klingeler, M. Loewenhaupt, and B. Büchner, *EPL* **88**, 37002 (2009).

¹⁴T. Masuda, A. Zheludev, A. Bush, M. Markina, and A. Vasiliev, *Phys. Rev. Lett.* **92**, 177201 (2004).

¹⁵S.-L. Drechsler, J. Málek, J. Richter, A. S. Moskvina, A. A. Gippius, and H. Rosner, *Phys. Rev. Lett.* **94**, 039705 (2005).

¹⁶T. Masuda, A. Zheludev, A. Bush, M. Markina, and A. Vasiliev, *Phys. Rev. Lett.* **94**, 039706 (2005).

¹⁷A. A. Gippius, E. N. Morozova, A. S. Moskvina, A. V. Zalesky, A. A. Bush, M. Baenitz, H. Rosner, and S.-L. Drechsler, *Phys. Rev. B* **70**, 020406 (2004).

¹⁸T. Masuda, A. Zheludev, B. Roessli, A. Bush, M. Markina, and A. Vasiliev, *Phys. Rev. B* **72**, 014405 (2005).

¹⁹H. Rosner, R. R. P. Singh, W. H. Zheng, J. Oitmaa, S.-L. Drechsler, and W. E. Pickett, *Phys. Rev. Lett.* **88**, 186405 (2002).

²⁰A. A. Tsirlin and H. Rosner, *Phys. Rev. B* **79**, 214416 (2009).

- ²¹O. Janson, J. Richter, and H. Rosner, *Phys. Rev. Lett.* **101**, 106403 (2008).
- ²²O. Janson, J. Richter, P. Sindzingre, and H. Rosner, [arXiv:1004.2185](https://arxiv.org/abs/1004.2185) (unpublished).
- ²³C. Gros, P. Lemmens, K.-Y. Choi, G. Güntherodt, M. Baenitz, and H. H. Otto, *Europhys. Lett.* **60**, 276 (2002).
- ²⁴K. Koepnick and H. Eschrig, *Phys. Rev. B* **59**, 1743 (1999).
- ²⁵J. P. Perdew and Y. Wang, *Phys. Rev. B* **45**, 13244 (1992).
- ²⁶H. Eschrig, K. Koepnick, and I. Chaplygin, *J. Solid State Chem.* **176**, 482 (2003).
- ²⁷M. T. Czyżyk and G. A. Sawatzky, *Phys. Rev. B* **49**, 14211 (1994).
- ²⁸A. Albuquerque, F. Alet, P. Corboz, P. Dayal, A. Feiguin, S. Fuchs, L. Gamper, E. Gull, S. Gürtler, A. Honecker, R. Igarashi, M. Körner, A. Kozhevnikov, A. Läuchli, S. R. Manmana, M. Matsumoto, I. McCulloch, F. Michel, R. M. Noack, G. Pawłowski, L. Pollet, T. Pruschke, U. Schollwöck, S. Todo, S. Trebst, M. Troyer, P. Werner, and S. Wessel, *J. Magn. Magn. Mater.* **310**, 1187 (2007).
- ²⁹M. Schmitt, J. Málek, S.-L. Drechsler, and H. Rosner, *Phys. Rev. B* **80**, 205111 (2009).
- ³⁰M. Schmitt, A. A. Gippius, K. S. Okhotnikov, W. Schnelle, K. Koch, O. Janson, W. Liu, Y.-H. Huang, Y. Skourski, F. Weickert, M. Baenitz, and H. Rosner, *Phys. Rev. B* **81**, 104416 (2010).
- ³¹H. Rosner, H. Eschrig, R. Hayn, S.-L. Drechsler, and J. Málek, *Phys. Rev. B* **56**, 3402 (1997).
- ³²N. Nagasako, T. Oguchi, H. Fujisawa, O. Akaki, T. Yokoya, T. Takahashi, M. Tanaka, M. Hasegawa, and H. Takei, *J. Phys. Soc. Jpn.* **66**, 1756 (1997).
- ³³To prove that, we plotted the orbital-resolved DOS for individual atoms. The states corresponding to the O atoms bridging two Cu atoms in a dimer show a clearly planar character. For the O atoms linking two neighboring dimers, the contributions from O $2p_x$ and O $2p_z$ are comparable, because the O $2p_z$ states correspond to the O $2p_x$ states of the neighbor dimer while the states from O $2p_y$ are negligible.
- ³⁴The difference between U_{eff} and U_{3d} is discussed in A. A. Tsirlin and H. Rosner, *Phys. Rev. B* **81**, 024424 (2010).
- ³⁵J. B. Goodenough, *Phys. Rev.* **100**, 564 (1955).
- ³⁶J. Kanamori, *J. Phys. Chem. Solids* **10**, 87 (1959).
- ³⁷P. W. Anderson, *Phys. Rev.* **79**, 350 (1950).
- ³⁸A. A. Tsirlin and H. Rosner (unpublished).
- ³⁹O. Janson, W. Schnelle, M. Schmidt, Y. Prots, S.-L. Drechsler, S. K. Filatov, and H. Rosner, *New J. Phys.* **11**, 113034 (2009).
- ⁴⁰We should note, that a good fit to the experimental magnetic susceptibility is by no means an evidence that the model itself is correct since essentially different sets of parameters for the same spin lattice and even for different lattices can yield similar macroscopic magnetic behavior.
- ⁴¹For the ordered phase, anisotropy plays a crucial role. Since the simulated model is isotropic, the temperature range corresponding to the AFM ordered phase (below $T_N < 15$ K) was excluded from the fit.
- ⁴²Although LSDA+ U calculations yield numerical values for the ordered moments on Cu as well as O atoms, they cannot properly account for quantum fluctuations, crucial for low-dimensional systems. Thus, for a quasi-one-dimensional compound BaCu₂Si₂O₇ LSDA+ U calculations yield 0.68 μ_B for the Cu moment (Ref. 43), considerably overestimating the experimental value of 0.15 μ_B (Ref. 44).
- ⁴³S. Bertaina and R. Hayn, *Phys. Rev. B* **73**, 212409 (2006).
- ⁴⁴M. Kenzelmann, A. Zheludev, S. Raymond, E. Ressouche, T. Masuda, P. Böni, K. Kakurai, I. Tsukada, K. Uchinokura, and R. Coldea, *Phys. Rev. B* **64**, 054422 (2001).
- ⁴⁵A. W. Sandvik, *Phys. Rev. B* **56**, 11678 (1997).
- ⁴⁶For the nonfrustrated diopside spin lattice, the value of the saturation field depends on J_c and g , but is not affected by the J_d/J_c ratio, as long as J_d is FM.
- ⁴⁷K. H. Breuer, W. Eysel, and R. Müller, *Z. Kristallogr.* **187**, 15 (1989).
- ⁴⁸J. M. Law, C. Hoch, M.-H. Whangbo, and R. K. Kremer, *Z. Anorg. Allg. Chem.* **636**, 54 (2010).
- ⁴⁹M. Hase, K. Ozawa, and N. Shinya, *Phys. Rev. B* **68**, 214421 (2003).
- ⁵⁰M. Hase, N. Terada, H. S. Suzuki, H. Kitazawa, K. Ozawa, K. Kaneko, N. Metoki, M. Matsuda, and K. Kakurai, *J. Phys.: Conf. Ser.* **150**, 042051 (2009).
- ⁵¹G. Castilla, S. Chakravarty, and V. J. Emery, *Phys. Rev. Lett.* **75**, 1823 (1995).
- ⁵²M. Schmitt *et al.* (unpublished).
- ⁵³J. Richter, J. Schulenburg, and A. Honecker, *Quantum Magnetism* (Springer, New York, 2004), Chap. 2, pp. 85–153.
- ⁵⁴L. Siurakshina, D. Ihle, and R. Hayn, *Phys. Rev. B* **61**, 14601 (2000).
- ⁵⁵R. Nath, A. A. Tsirlin, E. E. Kaul, M. Baenitz, N. Büttgen, C. Geibel, and H. Rosner, *Phys. Rev. B* **78**, 024418 (2008).
- ⁵⁶E. V. Castro, N. M. R. Peres, K. S. D. Beach, and A. W. Sandvik, *Phys. Rev. B* **73**, 054422 (2006).